Online Supplemental Material

Supplemental Methods

Axonal length measurements. Cells were filled with biocytin (1–2 mg ml^{-1}) during whole-cell recording and subsequently fixed with 4% paraformaldehyde in 0.1 M phosphate-buffered saline. After washing, tissue sections were incubated with fluorescein isothiocyanate (FITC)-conjugated avidin-D (2 µl ml^{-1}; Vector Laboratories, Burlingame, CA, USA) and 0.3% Triton X-100 during 24 h at 4° C. Slices were embedded in Prolong Antifade Gold (Invitrogen). Fluorescence was analysed with two-photon microscopy using a pulsed titanium:sapphire laser (Chameleon-XR tuned to 790 nm; Coherent, Santa Clara, CA, USA) attached to a Zeiss LSM 510 that was equipped with a 40x/1.3 numerical aperture oil-immersion objective. The morphology of the axon was reconstructed from a stack of 60–100 images (voxel size, 0.1–0.2 µm in the x–y plane; 0.2–0.3 µm along the z-axis). The axon was then manually traced within the three-dimensional image stack using a filament tracing software (Imaris 4.5; Bitplane, Zürich, Switzerland), and the length of the axon was measured from its somatic point of origin. In some cells (n = 5 out of 37 cells) the axon could not be fully reconstructed from the fluorescence data. For these reconstructions, the axonal length was approximately estimated from the shortest distance between the tips of the recording pipettes using the IR-DIC images acquired during the experiments (Kole *et al.* 2007).

Modelling. Simulations were performed using NEURON 6.0 (Carnevale & Hines, 2006) running under GNU/Linux. A detailed compartmental cable model of a granule cell (cell 7 from Schmidt-Hieber *et al.* 2007) was used as a passive skeleton into which we inserted kinetic models of Na^+ and K^+ conductances previously determined

in mossy fibre boutons and granule cell somata (Engel & Jonas, 2005). The passive membrane properties were assumed to be uniform, with a specific membrane capacitance of 1 µF cm^{-2}, a specific membrane resistance of 36 kΩ cm^2 and a specific intracellular resistivity of 163 Ω cm (Schmidt-Hieber *et al.* 2007). Increasing axonal R_m to 60 kΩ cm^2 (Alle & Geiger, 2006) had only minor effects on initiation site and propagation velocity (data not shown). Na^+ and K^+ channels were implemented as Hodgkin-Huxley models (Hodgkin & Huxley, 1952). The Na^+ current density (I_{Na}) was calculated as $I_{Na} = \bar{g}_{Na} \cdot m^3 \cdot h \cdot (V - E_{Na})$, where E_{Na} is the Na^+ equilibrium potential (assumed to be +60 mV), V is the membrane potential and m and h are the activation and inactivation state variables, respectively. A noninactivating K^+ current density (I_K) was described by $I_K = \bar{g}_K \cdot n^4 \cdot (V - E_K)$, where E_K is the K^+ equilibrium potential (assumed to be -85 mV) and n is the activation state variable. For activation of Na^+ channels, m was calculated using the voltage-dependent rate constants (Engel & Jonas, 2005):

$\alpha_m (V) = -93.8\ ms^{-1} \cdot (V - 117.0\ mV) / \{\exp[-(V - 117.0\ mV) / 17.7\ mV] - 1\}$ and

$\beta_m (V) = 0.168\ ms^{-1} \cdot \exp[-(V - 12.0\ mV) / 23.3\ mV]$.

h was calculated using the following inactivation rates for Na^+ channels:

$\alpha_h (V) = 0.000354\ ms^{-1} \cdot \exp[-(V - 12.0\ mV) / 18.7\ mV]$ and

$\beta_h (V) = 6.63\ ms^{-1} / \{\exp[-(V + 5.68\ mV) / 13.3\ mV] + 1\}$.

n was calculated using the following activation rates for K^+ channels:

$\alpha_n (V) = 0.01\ ms^{-1} \cdot (-V - 55\ mV) / \{\exp[-(V + 55\ mV) / 10\ mV] - 1\}$ and

$\beta_n (V) = 0.125\ ms^{-1} \cdot \exp[-(V + 65\ mV) / 80\ mV]$.

To account for the 2-times slower Na^+ channel inactivation recorded in granule cell somata (Engel & Jonas, 2005), α_h and β_h in the soma and dendrites were scaled by a factor of 0.5. The reversal potential of the leak conductance was set to -85 mV.

The time step was set to 5 µs. Segment length was adjusted according to the "d_lambda rule" (Carnevale & Hines, 2006) as follows. The alternating current (AC) length constant λ_{AC} at 1 kHz was calculated for each section, and the number of segments per section (*nseg*) was increased until the length of segments was below 10% of λ_{AC}. To obtain estimates of the maximal Na^+ and K^+ conductance densities ($\bar{g}_{Na}$ and $\bar{g}_K$), a representative axon with a length of 24 µm, a proximal diameter of 1.8 µm and a terminal diameter of 0.25 µm was connected to the soma. During the initial 8 µm, the diameter decreased monotonically from 1.8 to 0.8 µm, corresponding to a representative axon hillock. A bleb (diameter: 2.5 µm; length: 3 µm) was added to the end of the axon. $\bar{g}_{Na}$ and $\bar{g}_K$ were then varied to minimise the sum of squared errors between the maximal slopes during the rising and decaying phases of simulated and experimentally measured APs, respectively. Minimisation was performed using Brent's principal axis algorithm built into NEURON. For synaptic simulations, an intact axon with a total length of 1 mm was used. Synaptic conductance changes were simulated using the sum of two exponential functions with τ_{rise} = 0.2 ms and τ_{decay} = 2.5 ms, a reversal potential of 0 mV and peak conductances ranging from 0.1 – 1 nS, as described previously (Schmidt-Hieber *et al.* 2007).

Supplemental Results

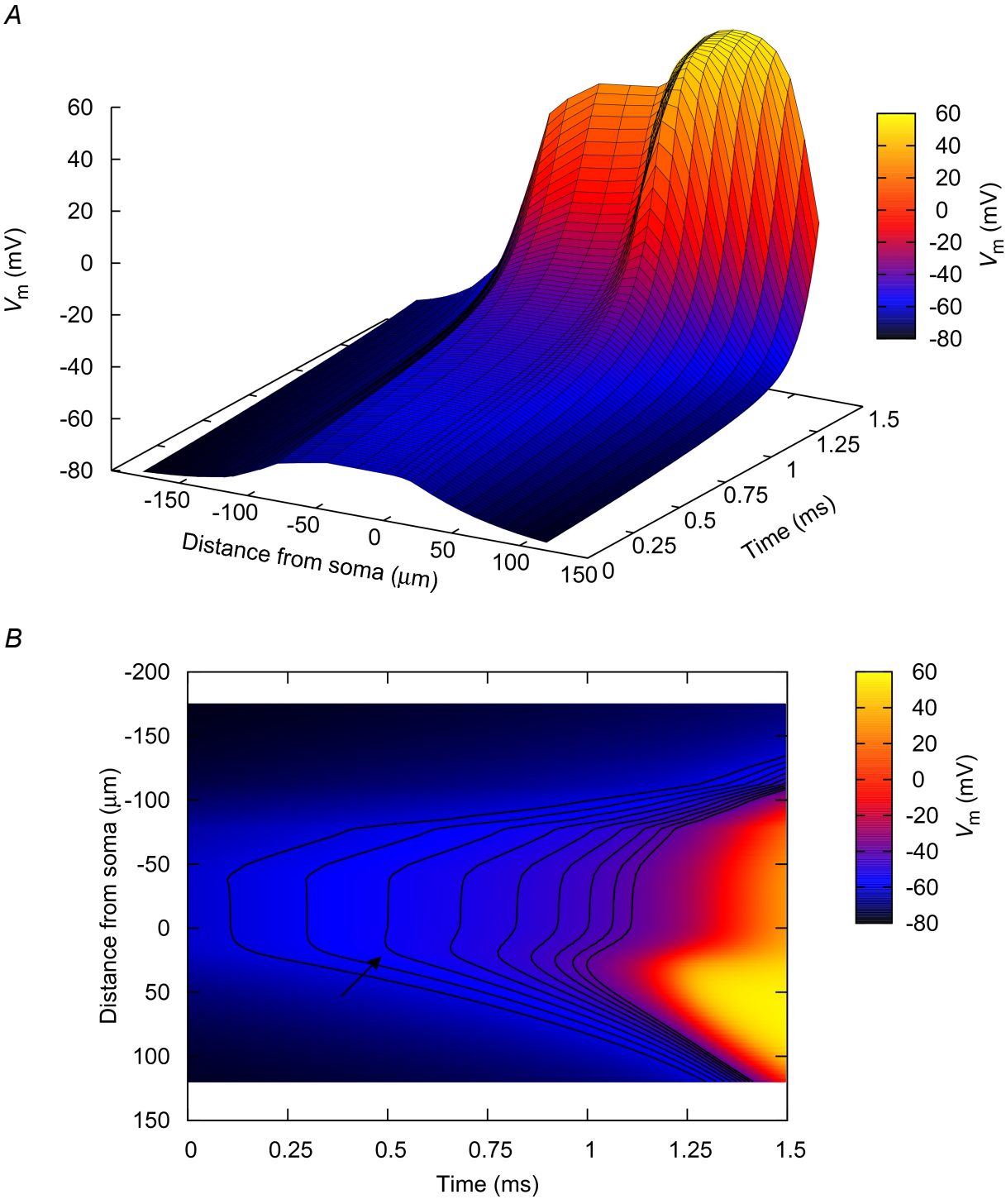

Supplemental Figure 1. Simulated APs are initiated in the proximal axon. *A*, Three-dimensional plot of the membrane potential V_m plotted against both time and distance from soma. Positive values denote the axon. In addition, membrane potential was colour-coded. The plot shows the initial rising phase of a simulated AP evoked by an excitatory synaptic conductance (same as in left panel of Fig. 4*E*). *B*, Density plot of the membrane potential V_m (colour-coded) which is plotted against both distance from soma and time (same AP as in *A*). The black contour lines indicate voltages between -60 mV to -40 mV in steps of 2.5 mV. Note that above a membrane potential of -55 mV (arrow), the voltage is always most positive in the initial part of the axon (at 20-30 µm from the soma).